Letters

IOP Publishing | Institute of Physics and Engineering in Medicine Physics in Medicine & Biology

Phys. Med. Biol. **62** (2017) L31–L40 https://doi.org/10.1088/1361-6560/aa84d7

Letter

Megahertz rate, volumetric imaging of bubble clouds in sonothrombolysis using a sparse hemispherical receiver array

Christopher N Acconcia[1,2], Ryan M Jones[1,2], David E Goertz[1,2], Meaghan A O'Reilly[1,2] and Kullervo Hynynen[1,2,3]

[1] Physical Sciences Platform, Sunnybrook Research Institute, Toronto, Canada
[2] Department of Medical Biophysics, University of Toronto, Toronto, Canada
[3] Institute of Biomaterials and Biomedical Engineering, University of Toronto, Toronto, Canada

E-mail: chrisacc@sri.utoronto.ca

Received 6 June 2017, revised 2 August 2017
Accepted for publication 8 August 2017
Published 5 September 2017

Abstract

It is well established that high intensity focused ultrasound can be used to disintegrate clots. This approach has the potential to rapidly and noninvasively resolve clot causing occlusions in cardiovascular diseases such as deep vein thrombosis (DVT). However, lack of an appropriate treatment monitoring tool is currently a limiting factor in its widespread adoption. Here we conduct cavitation imaging with a large aperture, sparse hemispherical receiver array during sonothrombolysis with multi-cycle burst exposures (0.1 or 1 ms burst lengths) at 1.51 MHz. It was found that bubble cloud generation on imaging correlated with the locations of clot degradation, as identified with high frequency (30 MHz) ultrasound following exposures. 3D images could be formed at integration times as short as 1 μs, revealing the initiation and rapid development of cavitation clouds. Equating to megahertz frame rates, this is an order of magnitude faster than any other imaging technique available for *in vivo* application. Collectively, these results suggest that the development of a device to perform DVT therapy procedures would benefit greatly from the integration of receivers tailored to bubble activity imaging.

Keywords: passive imaging, bubble cloud, sonothrombolysis, histotripsy

S Supplementary material for this article is available online

(Some figures may appear in colour only in the online journal)

1. Introduction

Vessel occlusions caused by blood clots can result in severe cardiovascular diseases such as ischemic stroke, myocardial infarction, and venous thromboembolism (VTE). VTE is the 3rd most common cardiovascular disease, annually affecting ~1 out of every 1000 individuals in North America and the European Union (Naess *et al* 2007, Go *et al* 2013). Deep vein thrombosis (DVT) accounts for the majority of patients with symptomatic VTE (White 2003) and can be fatal if left untreated, typically resulting from sequalae such as pulmonary embolism (PE). The standard treatment for DVT is anticoagulation therapy which reduces risk of embolization, further development of thrombus and thrombosis recurrence (Blum and Roche 2005). Although, anticoagulation therapy poorly addresses long-term morbidity following DVT. It is estimated that 20–50% of patients receiving anticoagulation develop post-thrombotic syndrome (PTS) (Prandoni *et al* 2004), significantly lowering quality of life (Kahn *et al* 2008). Alternative approaches directed at removing clots either by catheter-directed thrombolysis, mechanical thrombectomy, or both, result in better long-term outcome, reducing PTS (Avgerinos *et al* 2015, Haig *et al* 2016). However, these catheter-based approaches have limitations pertaining to potential incomplete clot removal (Comerota *et al* 2012), accessibility to patients in rural areas, and the invasive, time consuming nature of the procedure.

High intensity ultrasound can be used to disintegrate blood clots (Maxwell *et al* 2011a, Wright *et al* 2012), and is a promising approach to rapidly and non-invasively restore vessel patency in DVT. In the absence of lytic agents, clot degradation is attributed to the formation of a bubble cloud wherein the subsequent oscillation and collapse of bubbles can induce damage through a myriad of physical processes. Previous works have employed single-cycle (Zhang *et al* 2015c) and multi-cycle bursts (Wright *et al* 2012). Multi-cycle bursts involve a shock scattering mechanism of cloud formation (Maxwell *et al* 2011b) in which the cavitation cloud grows toward the acoustic source along the axis of acoustic propagation over the course of the burst. Bursts comprised of a single half cycle of the peak negative phase have been employed to avoid this shock scattering mechanism, confining the cavitation cloud to a smaller, more reproducible volume (Lin *et al* 2014). However, pre- or post-focal cavitation can still occur (Zhang *et al* 2015a) and avoidance of vessel damage is not guaranteed.

It is well established that cavitation inception depends on many factors (e.g. gas saturation of the medium, frequency, burst length, burst repetition frequency, peak negative pressure) and is a dynamic process that evolves rapidly over time (Maxwell *et al* 2011b). This emphasizes the requirement for a treatment monitoring technique to spatially identify where cavitation is occurring and to track its rapid temporal development. In work to date, bubble clouds have been imaged during sonothrombolysis with B-mode (Maxwell *et al* 2011a, Zhang *et al* 2015c) and color Doppler (Zhang *et al* 2015b) ultrasound. However, the frame rate with such approaches is low (~<100 Hz) relative to the timescale of the bubble dynamics (~1 MHz) and 3D imaging is not possible without a further reduction in frame rate. Acoustical passive imaging, on the other hand, is a technique to spatially map sources of acoustic emissions continuously by exploiting correlations of signals derived from an array of spatially distributed receivers (Sato and Sasaki 1977, Norton and Won 2000). This is frequently referred to as 'passive' since the receive array is not involved in exciting the medium and is an approach that is capable of high temporal resolution (e.g. Gyöngy and Coussios (2010b) and Jones *et al* (2013)) and therefore high frame rate imaging.

To date, all studies of passive cavitation imaging without incorporation of nucleation agents or preformed bubbles have used small aperture, linear arrays(e.g. Jensen *et al* (2012), Salgaonkar *et al* (2009), Gyöngy and Coussios (2010b) and Arvanitis and McDannold (2013)) including a recent report in the context of sonothrombolysis (Bader *et al* 2016). Without

mechanical translation or rotation, the use of linear arrays constrains imaging to 2D and small apertures provide limited spatial resolution due to the small acceptance angle of source signals. On the other hand, large aperture devices can achieve high spatial resolution (sub-millimeter) and 3D imaging when combined with 2D receiver arrays (O'Reilly and Hynynen 2013). These have been employed in the context of mapping cavitation from systemically injected microbubbles (Jones *et al* 2015, O'Reilly *et al* 2014, Deng *et al* 2016), but have yet to be investigated in the context of inertial cavitation type exposures without pre-formed cavitation nuclei.

In the work presented here, we employ a large aperture, sparse, hemispherical array to receive cavitation signals during inertial cavitation based sonothrombolysis. The objective is to assess the capabilities of passive imaging as a treatment monitoring tool with high temporal and spatial resolution using a near ideal receiver array geometry. The findings motivate and inform the design of a device for DVT treatment with receive elements for passive imaging being a key design aspect.

2. Materials and methods

2.1. General experimental approach

Blood clots were exposed to 1.51 MHz ultrasound and cavitation signals were received with a hemispherical array comprised of 128 sparsely populated, PZT elements each with a center frequency of 612 kHz and a diameter of 2.54 mm (see O'Reilly *et al* (2014) for details). Received signals were recorded for offline analysis. Conventional B-mode ultrasound imaging with a separate 1D imaging array is frequently employed to monitor for the presence of ultrasound induced cavitation clouds (Maxwell *et al* 2011a, Zhang *et al* 2015c). Here, contrast imaging was chosen over B-mode imaging for its specific detection of non-linear bubble scattering. Contrast image sequences were acquired at a frame rate of 28 Hz (i.e. 35.7 ms inter-frame time). The diagnostic probe (Phillips EPIQ, L12-5) was oriented to form images laterally spanning the axis of the vessel (figure 1). Following exposure, high frequency, 3D ultrasound imaging was performed to identify regions of clot degradation (Vevo 770, Visualsonics, Toronto, Canada). Remaining methods are described briefly in the following sections. For further details, see supplemental materials (stacks.iop.org/PMB/62/L31/mmedia).

2.2. Exposure conditions

Two exposure schemes were employed; long, 1 ms burst length exposures ($\times 60$) and short, 0.1 ms burst length exposures ($\times 100$) at a duty cycle of 0.1%. Long ($n = 3$) and short ($n = 4$) burst length exposures were conducted at peak negative pressures of ~8.5 and 15 MPa, respectively. In addition to single-site exposures, short duration bursts were conducted over multiple sites (5 sites, 1 mm intervals) to produce advanced erosion characteristics. Therapeutic bursts were delivered with an in-house manufactured, air backed, spherically focused transducer which had an aperture and focal length of 10 cm. The spatial extent of the pressure amplitude at the focus at -6 dB was 0.9 mm laterally, and 7.1 mm axially, measured with a fiber optic hydrophone (Precision Acoustics, United Kingdom, 10 μm diameter). The transducer was situated at 20° relative to the x-axis and positioned such that the focal point of the therapy transducer and the geometric focus of the hemispherical array coincided. This registration was achieved by focusing on a glass bead (Sigma-Aldrich, St. Louis, MO, USA, G1277, diameter ~200 μm) initially placed at the array's geometric focus.

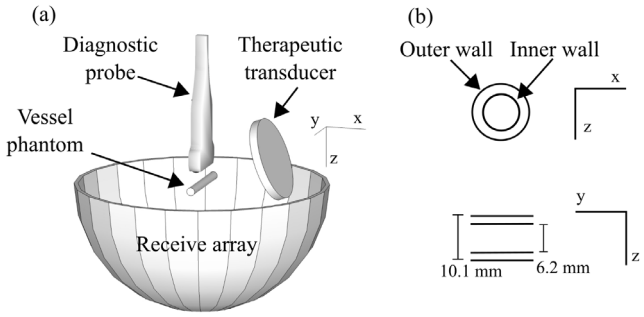

Figure 1. Schematic overview of the experimental apparatus (a) and cross-sectional views of the vessel phantom (b). The vessel housing the clot is shown at the geometric focus of the hemispherical receive array. The therapeutic transducer is oriented 20° relative to the x axis. Contrast images were formed in the yz plane.

2.3. Passive beamforming and data acquisition

Receive data was acquired at 40 MHz with a 128-channel receiver (SonixDAQ, BK Ultrasound, Richmond, BC, Canada) (Cheung *et al* 2012). Beamforming was conducted in the time domain using the time exposure acoustics algorithm (Norton and Won 2000). A 3D region of interest $10 \times 10 \times 10\,\text{mm}^3$ ($0.25\,\text{mm}^3$ voxel size) was selected for reconstructions centered on the geometric focus of the array. Raw data was digitally band-pass filtered between 500–700 kHz using a fourth order Butterworth filter. Beamforming was conducted with integration times, $\tau = 1$, 10 and 100 μs over moving, non-overlapping rectangular windows spanning ultrasound on-time, which equates to an imaging volume rate of up to 1 MHz. Similar to the approach taken by Haworth *et al* (2015), a relative intensity threshold level was identified from the time-averaged intensity of passive images that provided the best estimate of the size of the incurred bioeffects. Here, rather than evaluating the 1D spatial extent, we exploited the available 3D information to evaluate volumetric sizes. Once identified, the centroid of the volume within this threshold was compared to the region of clot degradation.

2.4. Clot formation

Blood was collected from pig femoral veins in vacutainer tubes containing sodium-citrate (Becton Dickinson & Co., Franklin Lakes, NJ, USA, 363083). Clotting was initiated with the addition of thrombin and calcium chloride following the work of Wright *et al* (2012). The vessel phantom (outer diameter 10.1 mm, inner diameter 6.2 mm) was made in-house using a urethane mold material (Tap Plastics Inc., CA, USA, Urethane RTV) that has been used in previous sonothrombolysis studies (Zhang *et al* 2015a, 2015c). The vessel was placed with the center coinciding with the geometric focus of the array, achieved by placing 2 glass beads on the vessel surface. These glass beads subsequently served as reference points for co-alignment of the cavitation images and high frequency ultrasound images.

3. Results

Bubble clouds generated with long (1 ms) and short (0.1 ms) burst length exposures were visualized with both passive and contrast imaging. Following exposures, the resultant clot degradation was clearly identifiable on 3D, high frequency ultrasound showing preferential damage of long and short duration exposures at the distal and proximal side of the vessel, respectively

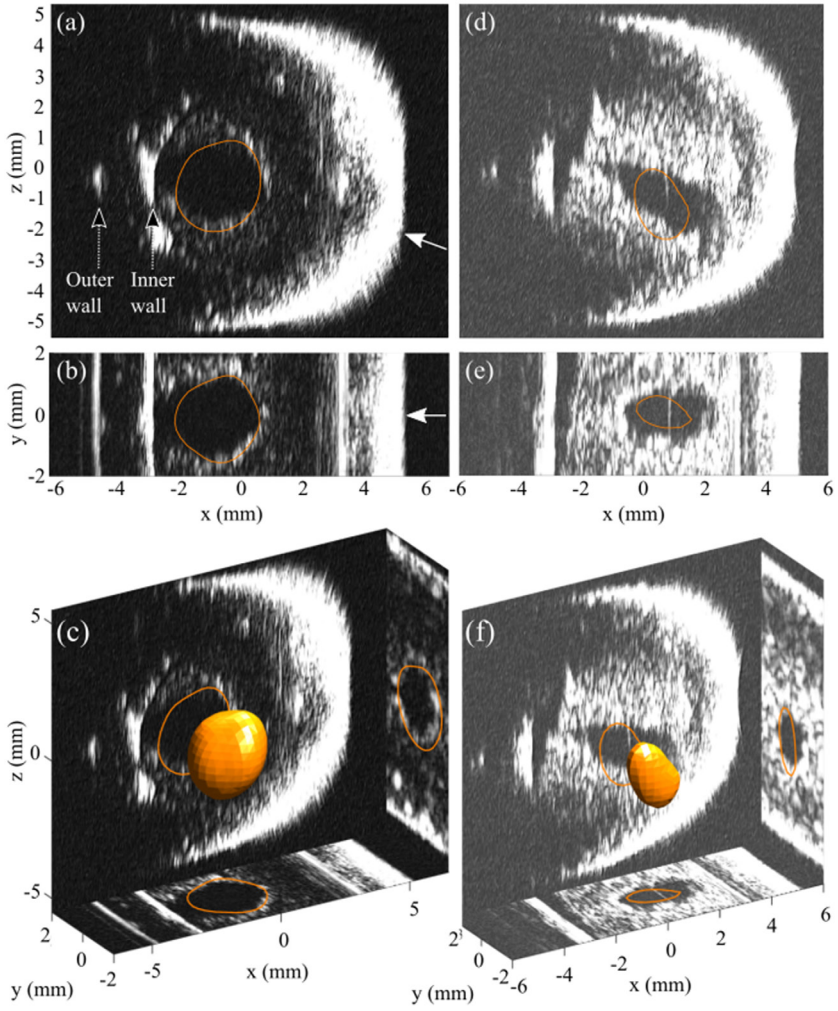

Figure 2. Time-averaged intensities at the −2 dB level overlayed on high frequency ultrasound images for long (a)–(c) and short (d)–(f) burst exposure sites. The contours in cross sectional views are shown as maximum intensity projections of the 3D surface of the −2 dB volume (c) and (f). Solid white arrows indicate the direction of acoustic propagation.

(figure 2). The spatial distribution of cavitation sources detected with passive imaging was consistent with that of clot degradation (see figure 2 and video 1 (stacks.iop.org/PMB/62/L31/mmedia)). Long duration bursts produced cavitation activity predominantly spanning from the focal zone to the post-focal zone whereas short duration exposures produced cavitation activity spanning from the focal zone to the pre-focal zone. From high frequency ultrasound, the volumes of degradation were $9.4 \pm 2.3\,\text{mm}^3$ and $4.2 \pm 2.4\,\text{mm}^3$ for long and short duration exposures, respectively. On passive imaging, the −2 dB level provided the best estimates of these degradation volumes, yielding corresponding volumes of $11.8 \pm 5.0\,\text{mm}^3$ and $2.1 \pm 0.8\,\text{mm}^3$. The centroids of the −2 dB volumes were contained within the volumes of degradation in all cases ($n = 7$).

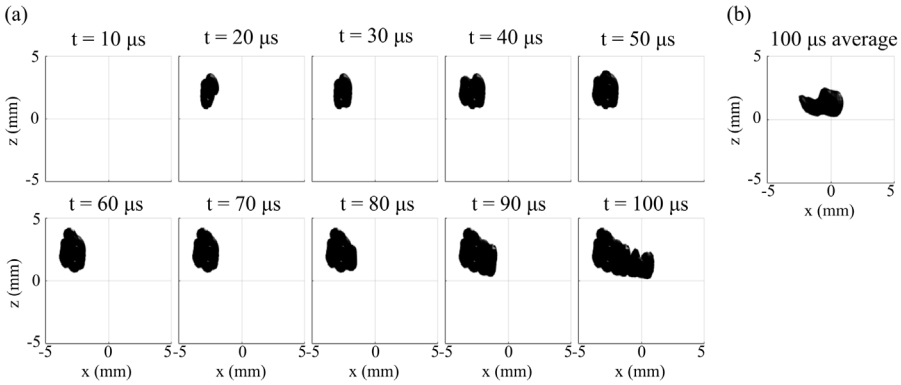

Figure 3. Reconstructed −2 dB volumes (viewed from an angle along the axis of the vessel) showing isolated sources over a single short duration burst for integration times of 1 μs (a) and 100 μs (b). Panel (a) presents every 10th frame with reconstructions from prior frames persisting. The 1 μs integration windows show the dynamic development of the bubble cloud on the microsecond timescale which can be overlooked with longer integration times. Initially, weak cavitation sources are present at the far vessel wall and towards the end of the burst the cloud rapidly develops, appearing at the center of the vessel, coinciding with the spatial maximum beamformed intensity reaching its temporal maximum over the burst. Data from burst number 13 of the sequence, the first burst in which the cloud appeared at the center of the vessel in passive imaging and could be identified on contrast imaging (see video 2 (stacks.iop.org/PMB/62/L31/mmedia) for passive imaging during this single burst and video 3 for the corresponding contrast imaging over the full exposure).

Integration times as short as 1 μs showed the rapid evolution of the bubble cloud and the stochastic nature of its dynamics. In comparison, 100 μs integration times failed to convey these microsecond timescale dynamics. Figure 3 shows data over a single burst from a short duration exposure site processed with integration times of 1 and 100 μs. The 1 μs integration time indicated isolated cavitation sources initially present at the distal vessel wall. Subsequently, the bubble cloud rapidly developed towards the center of the vessel at the end of the burst, coinciding with the beamformed intensity reaching its maximum value over the burst. In comparison, the 100 μs integration window only conveyed the cavitation cloud over the portion of time in which the largest acoustic signal was produced.

Only after several bursts was a bubble cloud identifiable on contrast imaging (e.g. video 3 (stacks.iop.org/PMB/62/L31/mmedia)). The number of bursts required were 13 ± 18 and 23 ± 9 for the long and short duration exposures, respectively. In the case of the multi-site short duration exposure, the number of bursts for each site was 30, 13, 25, 18, and 21. In all experiments, cloud appearance on contrast imaging coincided with the detection of cavitation sources at the center of the vessel under passive imaging. Prior to this occurring, passive imaging indicated the presence of cavitation sources distal and proximal to the center of the vessel along the acoustic propagation axis (e.g. video 2). After formation, the cloud appeared to grow with successive bursts under passive and contrast imaging. In addition, for the multi-site short duration exposure case, each sequential exposure site produced a bubble cloud with a greater extent in the direction of the previous site (figure 4). Contrast imaging also indicated that the cloud could persist between bursts. Following the exposure sequence the cloud persistence times were 1.9 ± 0.8 s and 1.2 ± 1.3 s for the long and short duration exposures, respectively.

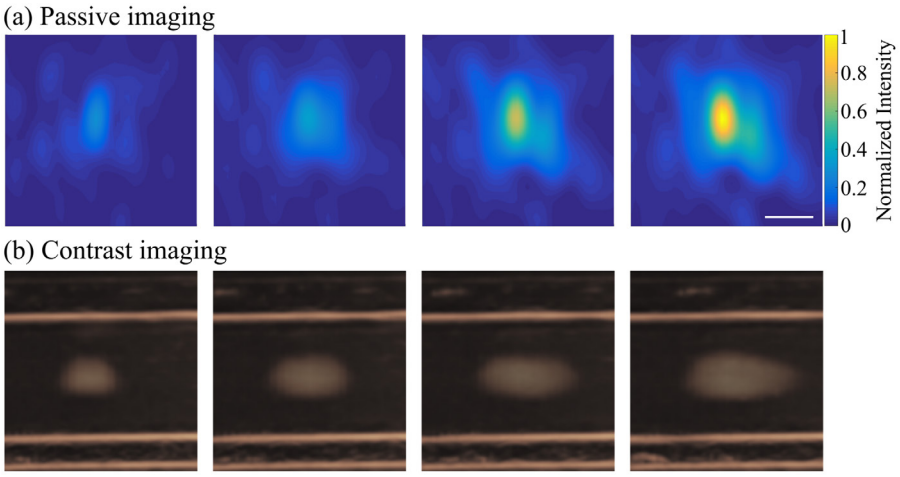

Figure 4. Cloud growth over sequential sites of sonication as observed in passive imaging (row (a)) and contrast imaging (row (b)). Each column corresponds to data from a different site conveyed as a sum projection over time. Passive images were additionally subject to sum projections along the *x*-direction (into the page) spanning 1.5 mm about the center of the vessel for a more direct comparison with the ~1.5 mm ultrasound imaging slice thickness. Data from short duration exposure sites, each separated by 1 mm (scale bar is 25 mm).

4. Discussion

A primary feature distinguishing passive imaging from other imaging techniques is the combination of both high frame rate and 3D imaging. In comparison, the frame rate of conventional contrast or B-mode imaging is currently limited to hundreds of Hz, and advanced US imaging techniques such as plane wave imaging can achieve frame rates of tens of kHz depending on compromises made in terms of image quality. Aside from being orders of magnitude lower than the frame rate capabilities of passive imaging, 3D B-mode imaging is currently not possible without a concomitant reduction in frame rate (~tens of Hz). The combined spatial and temporal evolution of bubble clouds is currently not well understood. Passive imaging is a tool which can provide insight into this evolution and to do so requires a temporal resolution on the timescale of the bubble dynamics (~microseconds), which equates to megahertz frame rates. The effective frame rate of passive imaging is limited primarily by considerations of the signal-to-noise ratio (SNR) of the system. Shorter integration times produce lower image SNR and higher peak side lobe to main lobe ratios for a given imaging array which can ultimately inhibit spatially isolated sources from being correctly identified. For stationary, harmonic point sources, increasing the integration time acts to reduce the receiver noise level, and the resulting side lobe pattern approaches the limiting case dictated by the array's diffraction pattern (Jones *et al* 2013). The results presented here showed that by using a hemispherical array of 128 narrowband receivers the SNR of the system was adequate to identify isolated sources at integration times down to 1 μs and that long integration times (i.e. low frame rates) can result in missing important details in the development of the bubble cloud (e.g. figure 3). Furthermore, the 4D information provided by passive imaging enabled detection of cavitation sources that would have otherwise been neglected. For example, prior to cavitation cloud appearance at the center of the vessel, sources were identified at the vessel walls, the detection of which could be important to avoid vessel damage *in vivo*. Presumably, the likelihood of

incurring vessel damage is related to the resident time of sources at the vessel walls, which could be more accurately assessed with higher volumetric rates. Notably, had the contrast imaging probe been used for passive imaging in the same orientation, the resultant 2D images would have also failed to detect these events.

Aside from the volume rate capabilities of the system, the large aperture of the receiver array provided high spatial resolution that enabled localization of cavitation sources within clot degradation volumes. Primarily, this owes to the receiver array's large acceptance angle of signals arising from sources close to the geometric focus. This results in a small point spread function (PSF) which was previously measured for the device at ~612 kHz to be ~1.3 mm laterally, and 2.7 mm axially (O'Reilly *et al* 2014). By comparison, at the same frequency, the theoretical PSF (Gyöngy and Coussios 2010a) of the small aperture linear array used in Bader *et al* (2016), is ~11 mm axially which would have likely hindered the ability to determine if cavitation energy was localized within the vessel or vessel wall were it used in the present study. Despite the small PSF of the system used here, there were still discrepancies between the degradation volume and that derived from passive imaging. In part, this can be attributed to the chosen metric of volume estimation. For example, once the clot has been damaged, much of the cavitation detected could be coming from bubbles at the core that are no longer involved in incurring damage. The signal strength of these sources is then less meaningful for volume estimates. It is also worth noting that the chosen metric for clot degradation volume/size estimation did not leverage the high volumetric rates presented as it was based on the time-averaged intensity over all bursts. Investigation into alternative metrics and evaluation of them with more rigorous volumetric analyses is warranted and will be a topic of future work.

A finding unique to contrast imaging was the persistence of the bubble cloud between bursts. This persistence of cavitation nuclei is useful information for treatment monitoring as so-called 'cavitation memory' effects have been proposed to influence treatment efficacy in sonothrombolysis (Zhang *et al* 2016) and soft-tissue fractionation (Duryea *et al* 2015). In the present work the persistence of bubbles could not be assessed with passive imaging since any potential residual cavitation nuclei were excited with the same exposures that generated bubble clouds. Incorporation of diagnostic type pulses (i.e. lower amplitude, shorter duration bursts) could be interleaved with therapeutic bursts to probe for residual nuclei and will be an aspect for future work.

The increasing spatial extent of the cloud at sequential sites was present in both passive images and contrast images. That multiple bursts were required to generate the cloud at each site suggests that it was not due to residual bubbles. Instead, bubbles could have been transported into the overlapping volume of degradation produced by previous exposures (for example due to radiation forces or fluid streaming). Indeed, the gradual migration of sources was observed in passive images (not shown here), supporting this explanation. In comparison with contrast imaging the lateral cloud dimensions were similar (figure 4), though the axial extent of the cloud on passive imaging appeared larger. However, direct comparisons between these two modalities should be made with caution. Firstly, due to the long inter-frame time (35.7 ms) relative to the burst durations (1 ms and 0.1 ms), contrast images are primarily formed between rather than during therapeutic bursts. Secondly, contrast imaging could only produce images of the cloud within a slice of finite thickness, centered on the vessel.

An important aspect of this work which aided in the interpretation of cavitation images and relating them to therapeutic effects was 3D high frequency imaging of the vessel phantom and the clot within it. Implicit here was the assumption that the vessel and/or clot had not significantly displaced or deformed during the time spanning the acquisition of cavitation signals. This would have complicated data processing and suggests that in order to fully take advantage of the megahertz volume rate capabilities of passive imaging would require concurrent structural imaging on timescales over which large displacements (relative to the PSF of the

system) are anticipated to occur. For example, this might be particularly relevant to cases in which vessels are unconstrained and exposed with long burst lengths.

Having leveraged the large aperture of a hemispherical receiver array, the results indicated that monitoring of sonothrombolysis would benefit from passive imaging. Though the array geometry of the device used here is well suited for transcranial applications such as ischemic stroke, alternative geometries would need to be considered for application in DVT (e.g. a half cylinder array geometry (Smirnov and Hynynen 2017)). The findings motivate for the development of a device tailored to this clinical application. Part of future work will be to conduct simulation studies to aid in the design of a device to optimize the configuration of receive elements as was conducted for the transcranial device used in this work (Jones *et al* 2013).

5. Conclusions

The results of this work present the capabilities of passive imaging for monitoring sonothrombolysis with a nearly ideal receiver array configuration. Cavitation sources were identified at megahertz frame rates and cavitation energy was largely localized within the core of clot degradation. The benefit of imaging at megahertz volume rates likely depends on the application in regards to the timescale over which the physical phenomena under study occur. In cases such as sonothrombolysis, where there is a rapidly developing cloud, the results suggest that imaging with high spatial resolution on the timescale of the bubbles dynamics is important.

Acknowledgment

This work was financially supported by a Canadian Institutes of Health Research (CIHR, grant no. MOP 142181) and Canada Research Chair Program.

References

Arvanitis C D and McDannold N 2013 Integrated ultrasound and magnetic resonance imaging for simultaneous temperature and cavitation monitoring during focused ultrasound therapies *Med. Phys.* **40** 112901

Avgerinos E D, Hager E S, Naddaf A, Dillavou E, Singh M and Chaer R A 2015 Outcomes and predictors of failure of thrombolysis for iliofemoral deep venous thrombosis *J. Vasc. Surg. Venous Lymphat. Disord.* **3** 35–41

Bader K B, Haworth K J, Shekhar H, Maxwell A D, Peng T, McPherson D D and Holland C K 2016 Efficacy of histotripsy combined with rt-PA *in vitro Phys. Med. Biol.* **61** 5253–74

Blum A and Roche E 2005 Endovascular management of acute deep vein thrombosis *Am. J. Med.* **118** 31S–6S

Cheung C, Yu A, Salimi N, Yiu B, Tsang I, Kerby B, Azar R and Dickie K 2012 Multi-channel pre-beamformed data acquisition system for research on advanced ultrasound imaging methods *IEEE Trans. Ultrason. Ferroelectr. Freq. Control* **59** 243–53

Comerota A J, Grewal N, Martinez J T, Chen J T, Disalle R, Andrews L, Sepanski D and Assi Z 2012 Postthrombotic morbidity correlates with residual thrombus following catheter-directed thrombolysis for iliofemoral deep vein thrombosis *J. Vasc. Surg.* **55** 768–73

Deng L, Reilly M A O, Jones R M, An R and Hynynen K 2016 A multi-frequency sparse hemispherical ultrasound phased array for microbubble-mediated transcranial therapy and simultaneous cavitation mapping *Phys. Med. Biol.* **61** 8476–501

Duryea A P, Roberts W W, Cain C A and Hall T L 2015 Removal of residual cavitation nuclei to enhance histotripsy erosion of model urinary stones *IEEE Trans. Ultrason. Ferroelectr. Freq. Control* **62** 896–904

Go A S *et al* 2013 Heart disease and stroke statistics—2013 update: a report from the american heart association *Circulation* **127** e6–245

Gyöngy M and Coussios C-C 2010a Passive cavitation mapping for localization and tracking of bubble dynamics *J. Acoust. Soc. Am.* **128** EL175–80
Gyöngy M and Coussios C-C 2010b Passive spatial mapping of inertial cavitation during HIFU exposure *IEEE Trans. Biomed. Eng.* **57** 48–56
Haig Y *et al* 2016 Post-thrombotic syndrome after catheter-directed thrombolysis for deep vein thrombosis (CaVenT): 5 year follow-up results of an open-label, randomised controlled trial *Lancet. Haematol.* **3** e64–71
Haworth K J, Salgaonkar V A, Corregan N M, Holland C K and Mast T D 2015 Using passive cavitation images to classify high-intensity focused ultrasound lesions *Ultrasound Med. Biol.* **41** 2420–34
Jensen C R, Ritchie R W, Gyöngy M, Collin J R T, Leslie T and Coussios C-C 2012 Spatiotemporal monitoring of high-intensity focused ultrasound therapy with passive acoustic mapping *Radiology* **262** 252–61
Jones R M, O'Reilly M and Hynynen K 2013 Transcranial passive acoustic mapping with hemispherical sparse arrays using CT-based skull-specific aberration corrections: a simulation study *Phys. Med. Biol.* **58** 4981–5005
Jones R M, O'Reilly M and Hynynen K 2015 Experimental demonstration of passive acoustic imaging in the human skull cavity using CT-based aberration corrections *Med. Phys.* **42** 4385–400
Kahn S R *et al* 2008 Determinants of health-related quality of life during the 2 years following deep vein thrombosis *J. Thromb. Haemost.* **6** 1105–12
Lin K W, Kim Y, Maxwell A, Wang T Y, Hall T, Xu Z, Fowlkes J and Cain C 2014 Histotripsy beyond the intrinsic cavitation threshold using very short ultrasound pulses: microtripsy *IEEE Trans. Ultrason. Ferroelectr. Freq. Control* **61** 251–65
Maxwell A D, Owens G, Gurm H S, Ives K, Myers D D and Xu Z 2011a Noninvasive treatment of deep venous thrombosis using pulsed ultrasound cavitation therapy (histotripsy) in a porcine model *J. Vasc. Interv. Radiol.* **22** 369–77
Maxwell A D, Wang T-Y, Cain C A, Fowlkes J B, Sapozhnikov O A, Bailey M R and Xu Z 2011b Cavitation clouds created by shock scattering from bubbles during histotripsy *J. Acoust. Soc. Am.* **130** 1888–98
Naess I A, Christiansen S C, Romundstad P, Cannegieter S C, Rosendaal F R and Hammerstrøm J 2007 Incidence and mortality of venous thrombosis: a population-based study *J. Thromb. Haemost.* **5** 692–9
Norton S J and Won I J 2000 Time exposure acoustics *IEEE Trans. Geosci. Remote Sens.* **38** 1337–43
O'Reilly M and Hynynen K 2013 A super-resolution ultrasound method for brain vascular mapping *Med. Phys.* **40** 110701
O'Reilly M A, Jones R M and Hynynen K 2014 Three-dimensional transcranial ultrasound imaging of microbubble clouds using a sparse hemispherical array *IEEE Trans. Biomed. Eng.* **61** 1285–94
Prandoni P, Lensing A, Prins M, Frulla M, Marchiori A, Bernardi E, Tormene D, Mosena L, Pagnan A and Girolami A 2004 Below-knee elastic compression stockings to prevent the post-thrombotic syndrome *Ann. Intern. Med.* **141** 249–56
Salgaonkar V A, Datta S, Holland C K and Mast T D 2009 Passive cavitation imaging with ultrasound arrays *J. Acoust. Soc. Am.* **126** 3071–83
Sato T and Sasaki K 1977 Bispectral holography *J. Acoust. Soc. Am.* **62** 404–8
Smirnov P and Hynynen K 2017 Design of a HIFU array for the treatment of deep venous thrombosis: a simulation study *Phys. Med. Biol.* **62** 6108–25
White R 2003 The epidemiology of venous thromboembolic disease venous thromboembolism *Circulation* **107** 4–9
Wright C, Hynynen K and Goertz D 2012 *In vitro* and *in vivo* high-intensity focused ultrasound *Invest. Radiol.* **47** 217–25
Zhang X, Jin L, Vlaisavljevich E, Owens G E, Gurm H S, Cain C A and Xu Z 2015a Noninvasive thrombolysis using microtripsy: a parameter study *IEEE Trans. Ultrason. Ferroelectr. Freq. Control* **62** 2092–105
Zhang X, Miller R M, Lin W-L, Levin A M, Owens G E, Gurm H S, Cain C A and Xu Z 2015b Real-time feedback of histotripsy thrombolysis using bubble-induced color Doppler *Ultrasound Med. Biol.* **41** 1386–401
Zhang X, Owens G E, Cain C A, Gurm H S, Macoskey J and Xu Z 2016 Histotripsy thrombolysis on retracted clots *Ultrasound Med. Biol.* **42** 1903–18
Zhang X, Owens G E, Gurm H S, Ding Y, Cain C A, Arbor A, Diseases C, Arbor A and Arbor A 2015c Non-invasive thrombolysis using histotripsy beyond the 'intrinsic' threshold (microtripsy) *IEEE Trans. Ultrason. Ferroelectr. Freq. Control* **62** 1342–55